

# Multiband Metamaterial Absorber Design Based on Plasmonic Resonances for Solar Energy Harvesting

Batuhan Mulla<sup>1</sup> · Cumali Sabah<sup>2</sup>

Received: 25 October 2015 / Accepted: 30 December 2015 / Published online: 13 January 2016  
© Springer Science+Business Media New York 2016

**Abstract** A new metamaterial absorber is designed and characterized numerically for the harvesting of solar energy. The design is composed of three layers in which the interaction among them gives rise to the plasmonic resonances. The main operation frequency range of the proposed structure is chosen to be the visible regime. However, the design is also analyzed for the infrared and ultraviolet regimes. In order to characterize the absorber, some parametric studies with respect to the dimensions of the structure are carried out. According to the results, it is found that the proposed metamaterial absorber has 98.2 % absorption capability at 445.85 THz and 99.4 % absorption capability between 624 and 658.3 THz. Moreover, the polarization dependency of the structure is examined and it is found that the design operates well as a perfect absorber with polarization independency for the studied frequency range. As a result, the proposed metamaterial absorber can be used for solar energy harvesting as it provides multiple perfect absorption bands in the visible regime.

**Keywords** Metamaterial · Perfect absorption · Multiband · Solar energy · Energy harvesting

## Introduction

Interesting, exotic, and unavailable behaviors of metamaterials like double negativity [1, 2] (which creates negative refraction) caused the researchers to take attentions on metamaterials. Researches for metamaterials are being made for the different frequency realms such as gigahertz [3–5], terahertz [6–8], and optical [9–11] for many purposes such as perfect lenses, optical cloaking, energy harvesting, sensing, and perfect absorption [12–18]. Perfect absorption can be realized when these materials are engineered in a way that they neither transmit nor reflect the incident wave. Especially, for some of the applications of metamaterials, like micro-bolometers, sensors, thermal imagers, and solar energy utilization, perfect absorption property is essential [16–21].

Perfect absorption can be realized when the frequency-dependent effective impedance of the metamaterial absorber becomes the same with the impedance of free-space so that the reflected and transmitted waves reduces to zero [22]. In addition to these, excitation of the plasmon polaritons at terahertz frequencies can give rise to the plasmonic resonances to absorb the incident wave efficiently [23, 24]. The resonant frequency and the capability of metamaterial absorbers are highly dependent to the geometric parameters of the structure (as well as its chemical composition). By altering these parameters, the electrical and optical behavior of these kinds of plasmonic absorbers can easily be tuned [25].

Heat or thermal energy can be converted into usable forms of energy (mainly electricity) by the utilization of thermo-photovoltaics. These devices are the combination of an absorber/emitter, a photodiode, and an external heat source [21, 26]. The working mechanism of thermo-photovoltaics starts with the absorption and re-emission of the energy coming from the heat source. Re-emitted radiation can be used by the photovoltaic cells to convert solar or heat energy into the electricity.

---

✉ Cumali Sabah  
sabah@metu.edu.tr

<sup>1</sup> Sustainable Environment and Energy Department, Middle East Technical University—Northern Cyprus Campus, Kalkanli, Guzelyurt, TRNC / Mersin 10, Turkey

<sup>2</sup> Department of Electrical and Electronics Engineering, Middle East Technical University—Northern Cyprus Campus, Kalkanli, Guzelyurt, TRNC / Mersin 10, Turkey

Therefore, the absorption property of the metamaterial absorber can be used to capture the solar radiation by the integration of such absorbers into the photovoltaic and/or thermo-photovoltaic systems. In this sense, a metamaterial absorber can be used to improve the miniaturization and the efficiency of thermo-photovoltaics or photovoltaics.

Solar radiation covers the range between 100 and 1000 THz. However, most of the energy is located between 400 and 750 THz [27]. If a metamaterial absorber has a good absorption rate in this range, it can be utilized very efficiently for the solar energy harvesting (as opposed to the conventional absorber systems with a limited efficiency). Thus, some of the energy requirements of the human beings supplied by sun as renewable and sustainable sources can be increased with these original arrangements.

Most of the previous studies focused on only one frequency region, for example, Ayas et al. [9] worked on a metamaterial absorber structure which was designed to work in visible frequency range. Their design has three bands in this range. Liu et al. [28] designed an aluminum-based metamaterial absorber. Their absorber designed to operate in the ultraviolet frequency range. In addition, some of the studies in the literature focused on the multilayered absorber in order to absorb solar energy. Liang et al. [29] presented a metamaterial solar energy absorber which has a pyramidal shape. They utilized vertically cascaded metal-dielectric layers in order to obtain perfect absorption in the solar range. Moreover, Wu et al. [30] investigated the absorption effects in grating-based devices. Their structure is designed to operate in infrared frequencies. They also utilized vertically cascaded metal-dielectric grating for obtaining multiband absorption.

In this paper, a new metamaterial absorber design which is composed of a metallic ground plane, a dielectric spacer layer, and metallic resonators is introduced to absorb the solar energy effectively. The characterization of the resonators and analysis of the geometric parameters of the structure are carried out to understand the absorption mechanism of the proposed metamaterial absorber. According to the results, multiband (one being wide) perfect absorption is achieved in the visible realm.

## Design and Simulation

The geometry of the design is presented in Fig. 1. This absorber is composed of three layers: the continuous metallic bottom layer with the thickness “ $h$ ,” dielectric separator with the thickness “ $d$ ,” and the metallic resonator at the top of the structure with the thickness “ $e$ .” The resonator itself has different geometric configurations which can be expressed as corner patches, central patch, and strips. The geometric dimensions and the letters denoted to these dimensions are given in Fig. 1b while the values associated with each parameter are presented in Table 1. The unit cell periodicity of the proposed design is given by “ $p$ .” Each of the resonator pairs shown in Fig. 1 is responsible from the resonance at different frequencies.

The contribution of these resonators to the absorption spectrum will be discussed in the next section. The metallic parts of the structure are aluminum (Al) where the silicon dioxide (SiO<sub>2</sub>) is used as dielectric material. Aluminum has been chosen because of its relatively lower material cost and lower skin depth (especially when compared with silver and gold) which might reduce the total cost in practical applications. Frequency-dependent complex dielectric parameters of Al and SiO<sub>2</sub> are taken from Palik’s book [31].

In order to characterize the unit cell and understand the absorption mechanism of the design, some simulations are performed. Optimum parameters for the proposed metamaterial absorber are obtained by varying and simulating all the mentioned parameters in Table 1 simultaneously. These simulations are carried out by a commercial simulation software which uses finite integration technique to solve the Maxwell’s equations. Boundary conditions for the simulations are chosen to be periodic in  $x$  and  $y$  direction and open boundaries are used along  $z$  direction. In the numerical analysis, the electric and magnetic field components of the incident plane wave are assumed to be polarized in  $x$  and  $y$  direction, respectively. The direction of propagation is along the  $z$  direction, as shown in Fig. 1b.

Solar radiation covers the range between 100 and 1000 THz, from near infrared to ultraviolet region. Because of the higher solar irradiance in the visible frequency range, simulations are mainly carried out in this range. However, the reflectance and absorption spectra of the proposed absorber in the infrared and ultraviolet regions are also presented in the following sections.

As the bottom continuous Al metallic plate has the thickness greater than the skin depth, it acts like an optical mirror and prevents the transmissions to pass through the structure. Under these circumstances, transmission becomes negligible (approximately zero).

Optical absorption behavior of the proposed structure can be calculated by using Eq. 1 where the frequency dependent parameters  $A(\omega)$ ,  $R(\omega)$ , and  $T(\omega)$  represents the absorption reflectance and transmittance, in order. As it is mentioned before,  $T(\omega)$  can be neglected because of the optical preventative characteristics of the bottom Al plate. Therefore, Eq. 1 reduces to Eq. 2. Using the obtained scattering parameters ( $S_{11}$  and  $S_{21}$ ) from the simulations, the absorption can be calculated and plotted via Eq. 3.

$$A(\omega) = 1 - R(\omega) - T(\omega) \quad (1)$$

$$A(\omega) = 1 - R(\omega) \quad (2)$$

$$A(\omega) = 1 - |S_{11}|^2 \quad (3)$$

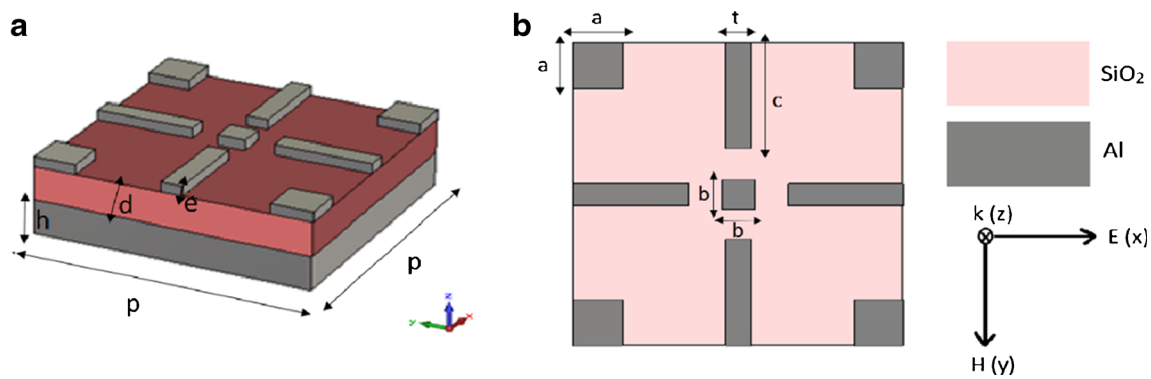


**Fig. 1** Geometry of the unit cell of the proposed metamaterial absorber structure. **a** Perspective view. **b** Front view

**Results and Discussion**

The introduced metamaterial absorber has three absorption resonances in the interested frequency range (visible region due to the high solar radiation level). The first absorption resonance occurred at 445.85 THz while the second and the third resonances take place at 624 and 658.3 THz, respectively. Note that, because the second and the third resonances are very close to each other, they formed a wide-band absorption with the bandwidth of 34.3 nm where the absorption rate is more than 99.4 % in this wide-band region. The absorption levels are 98.2, 99.8, and 99.9 % for the first, second, and third resonances, correspondingly. The absorption and reflectance spectra for the visible region are given in Fig. 2. The inserted plot represents the zoom of the absorption bands for the second and the third resonances.

In addition to visible frequency range, the absorption behavior of the metamaterial absorber is investigated in the ultraviolet and infrared frequency ranges. The obtained results for these ranges are given in Fig. 3. Figure 3a represents the spectra for infrared region while Fig. 3b displays the spectra for ultraviolet region. For infrared region, the absorption peak is obtained at 201.4 THz with the percentage of 81.4 %. This resonance can further be improved by altering the geometric dimensions of the structure as it is performed for the visible range in the following sections. For the ultraviolet region, the absorber does not provide any significant resonance peak. However, at the beginning of this region, the magnitude of the absorption is around 78 % and it is decreasing to 40 % at the end of this region. Therefore, it can be concluded that the proposed absorber not only absorbs the radiation in the visible range but also absorbs the radiation almost in all solar spectrum with different magnitudes.

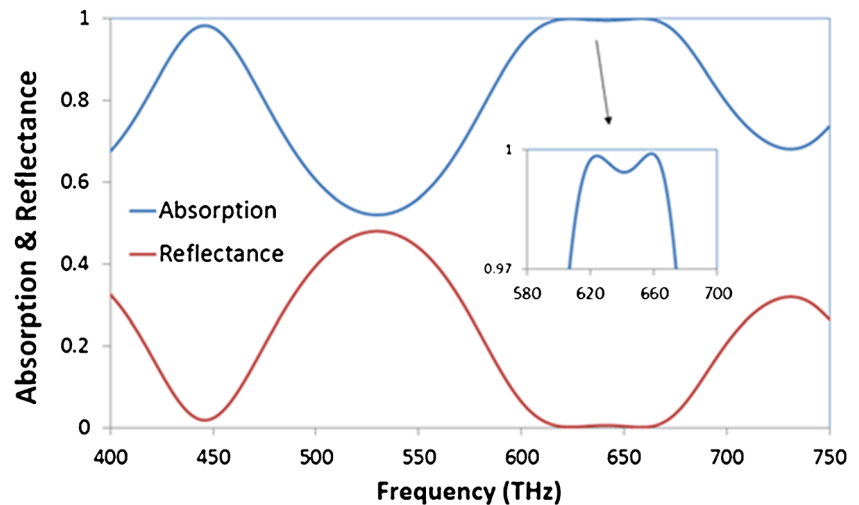
**Table 1** Values associated with each parameter in nanometer

Parameter	<i>p</i>	<i>a</i>	<i>c</i>	<i>b</i>	<i>H</i>	<i>d</i>	<i>e</i>	<i>t</i>
Value (nm)	400	40	140	60	50	50	15	30

In this part, the resonators of the structure have been divided into two groups in order to perform the characterization of these elements; the first group consists of the square patches at the corner and the second group composed of the combination of the strips and the square patch at the center of the unit cell. The individual responses of the mentioned groups are given in Fig. 4 (the first group is shown in Fig. 4a while the second group is in Fig. 4b). The first group is responsible from the dual-band absorption alone with perfect absorption in the visible regime caused by the interaction between the resonators and the bottom metallic plate (Fig. 4a) [9, 24]. Although, the resonators in the second group also provide two absorption bands alone (one being in the infrared and the other in visible range), the absorption rate provided by this group is nearly 80 % (Fig. 4b) for both of the resonances. However, when all of the resonators are combined, the absorption strength increases because of the coupling and plasmonic effects of the resonances. Here, the central square patch is added to the second group because it enhances the magnitude of the resonance provided by the strips in the visible range. Moreover, it also causes the shift in resonance wavelength as can be seen in Fig. 4c. Magnified resonance peaks can be seen in the inset of the Fig. 4c. The resonance wavelength takes place at 599.5 THz with the strength of 0.73, when only strips are used. However, when the strips and central patch are combined the the wavelength shifts to 603.7 THz and the strength increases to 0.78.

Moreover, the behavior of the resonances and the operation mechanism of the metamaterial absorber can be understood by analyzing the electric field, magnetic field, and surface current distributions at the resonant frequencies which are presented in Fig. 5. Here, the plots from (a<sub>1</sub>)-(c<sub>1</sub>) represents the *x*-component of the electric field distributions (*E<sub>x</sub>*), (a<sub>2</sub>)-(c<sub>2</sub>) represents the *z*-component of the electric field distributions (*E<sub>z</sub>*), (a<sub>3</sub>-c<sub>3</sub>) represents the magnitude of the electric field distributions (*|E|*), (a<sub>4</sub>)-(c<sub>4</sub>) represents the *y*-component of the magnetic field distributions (*H<sub>y</sub>*), and (a<sub>5</sub>)-(c<sub>5</sub>) represents the surface current distribution of proposed absorber at *f*=445.85 THz, *f*=624 THz, and *f*=658.3 THz, correspondingly. The scales of the corresponding distributions are given

**Fig. 2** The reflectance and absorption spectra of the structure in the visible frequency region



at the bottom of each group. At the first resonance of 445.85 THz, the electric field is mainly concentrated near the inner edges of the square patches at the corner and the sides of the strip in the middle ( $a_1$ - $a_2$ ). The concentration of electric field in the dielectric layer (Fig. 5a<sub>2</sub>) separates the positive and the negative charges so that the structure behaves like an electric dipole. Moreover, strong electric field distribution couples the resonators and the ground plane. The coupling between the corner square resonators and the ground plane comes out with the generation of the magnetic polaritons which creates antiparallel current distribution as shown in Fig. 5a<sub>4</sub> [7]. Therefore, for this resonance, it can be stated that the electric and magnetic polaritons are mainly caused by the square patches at the corner. Simultaneously formed electric and magnetic responses yield the impedance matching between the structure and free-space so that the perfect absorption is fulfilled. For the second resonance of  $f=624$  THz, two electric hot spots are located at the inner sides of two square rings which creates the electric response for this resonance. However, the magnetic response of the metamaterial absorber is caused by the circulating loops around the strip in the middle where the magnetic polaritons are formed. Moreover, the differences in the magnetic resonances between the first and the second resonances indicate

the different resonance modes. Note that the magnetic field is continuous and strong along the  $y$  direction. The distributions of the third resonance ( $f=658.3$  THz) can be seen in Fig. 5c<sub>1</sub>-c<sub>5</sub>. The electric field hot spots confined at the sides of the corner square patches and the middle of the structure. Such distribution created net electric dipole moment; therefore, the electric polaritons and electric resonance are formed. In addition, antiparallel currents caused by the circulating current loops provide the formation of magnetic resonance. Thus, this resonance can be attributed as the stronger version of the second resonance; hence, the fields are distributed as the same and stronger than the second resonance. Moreover, the magnitude of the electric field distributions ( $|E|$ ) at  $y$ - $z$  plane on the top of the dielectric layer for the three resonances (Fig. 5a<sub>3</sub>-c<sub>3</sub>) supports the previously discussed comments related with the resonances.

In the next step, the dependence of the absorption peaks to the geometric parameters is examined. Keeping the other parameters fixed, dielectric layer thickness (parameter  $d$ ), resonator thickness (parameter  $e$ ), strip length (parameter  $c$ ), and strip width (parameter  $t$ ) are altered for characterization and better understanding the mechanism of the absorber. In order to obtain the optimum parameters for the proposed metamaterial absorber, all the mentioned parameters are

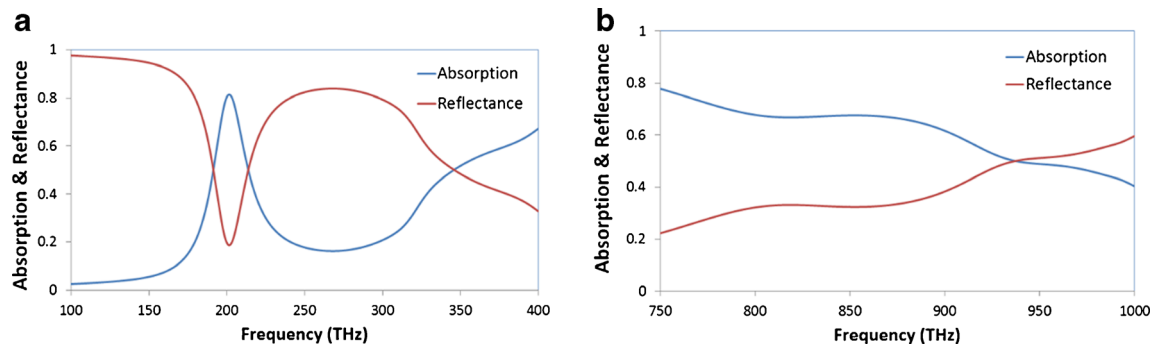


**Fig. 3** The reflectance and absorption spectra of the structure **a** in infrared frequency region and **b** in ultraviolet frequency region

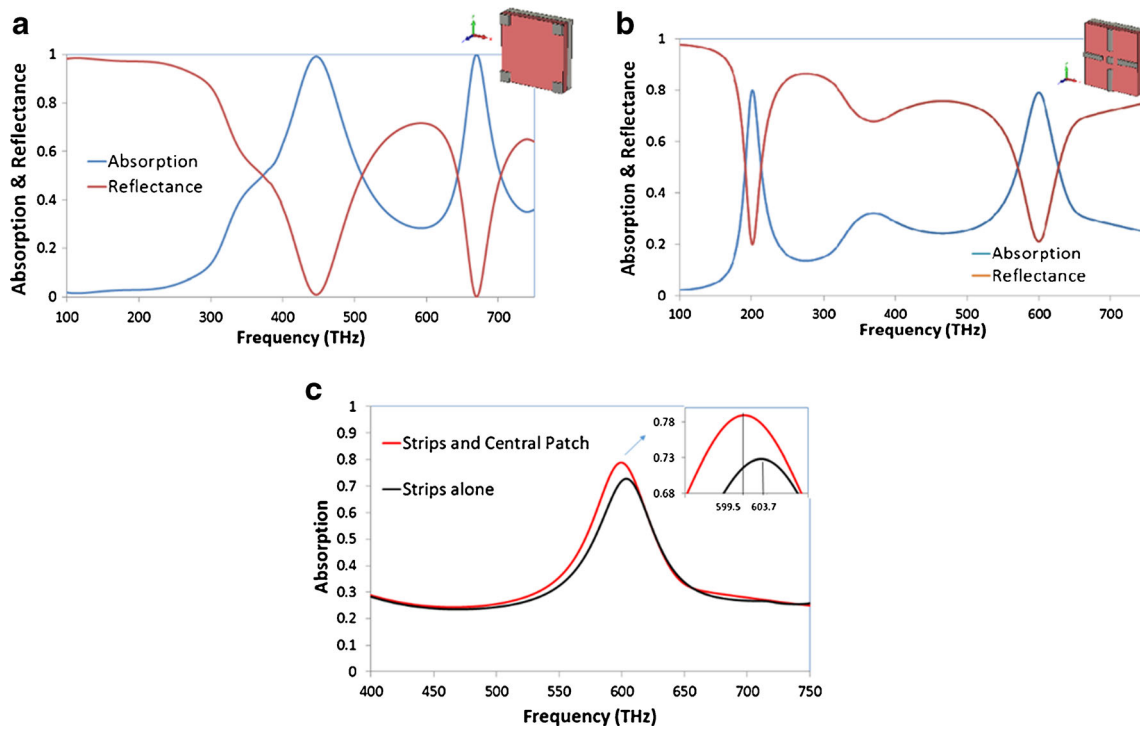


**Fig. 4** The contribution of the resonators to the absorption spectrum. **a** The contribution of the patches at the corners and **b** the contribution of the strips and the patch at the central of the structure. **c** Comparison of the effects of the central patch on the absorption spectrum

changed and simulated simultaneously. Results for the mentioned parametric studies are given in Fig. 6. Note that the red curves in all plots indicate the desired results with respect to the absorption rate and those parameters can be selected as the optimum parameters for the perfect absorption.

First, the thickness of the dielectric layer is examined. The effect of the dielectric thickness to the resonant frequency and absorption rate is observed by altering parameter  $d$ . The response is given in Fig. 6a. The optimum thickness for the dielectric layer is found to be  $d = 50$  nm. The dielectric thickness mainly helps the coupling between the electric resonance occurred on the metallic resonators with the bottom metallic layer. Thus, this coupling creates a magnetic response and finally makes the effective impedance of the absorber to be equal to the impedance of the free-space (impedance matching). This situation was also verified by the electric and magnetic distributions given in Fig. 5. Although, the thickness of the dielectric separation is enough to create a magnetic response for the  $d$  smaller and greater than 50 nm, it does not provide the impedance matching for some thicknesses. Thus, the selection of the dielectric thickness for such structures is very important to have perfect absorption.

Resonator thickness ( $e$ ) is one of the other important parameter that determines the absorption strength/rate and resonant frequency. The variation can be seen in Fig. 6b. As can be seen from the figure, the structure gives only one resonance at around 650 THz when thin resonators are used. However, when the thicknesses are increased, the magnitude of the absorption is enhanced at three different frequency locations of

the visible frequency region for different thicknesses. When  $e$  is adjusted to the small values (like 5 nm), the thickness of the resonator becomes not enough to generate the perfect absorber response caused by the metallic resonators. However, when the thickness is higher than a certain value (such as 20 nm), the structure reflects some part of the incident wave. If the thickness continued to be increased, the metallic parts start to behave like an optical mirror (results not shown here). Therefore, for the proposed structure,  $e = 15$  nm can be selected for the perfect absorption which has a good harmony between the transmitted and reflected waves (almost zero reflection and transmission) and also creates the desired electric and magnetic responses.

As can be seen from Fig. 6c, the resonances are also dependent on the length of the strips (parameter  $c$ ). Although the first resonance at 445.85 THz is not affect from the changes at parameter  $c$ , the second and the third resonances are strongly dependent on this parameter. This is expected because the electric and magnetic responses depend on the resonators of the first group (not the strips: second group) at the first resonance as can be seen in Fig. 5a<sub>1</sub>-a<sub>4</sub>. As discussed in the previous section, the third resonance is contributed by the square patches at the corner when all the resonators are qualified separately. However, when all the resonators combined in a unit cell, the individual resonators or the groups of resonators can affect each other. Therefore, in Fig. 6c, it can be seen that the third resonance is affected from the strip length. This is mainly because of the interactions between the resonator elements. Therefore, by altering the length, the ideal case for the

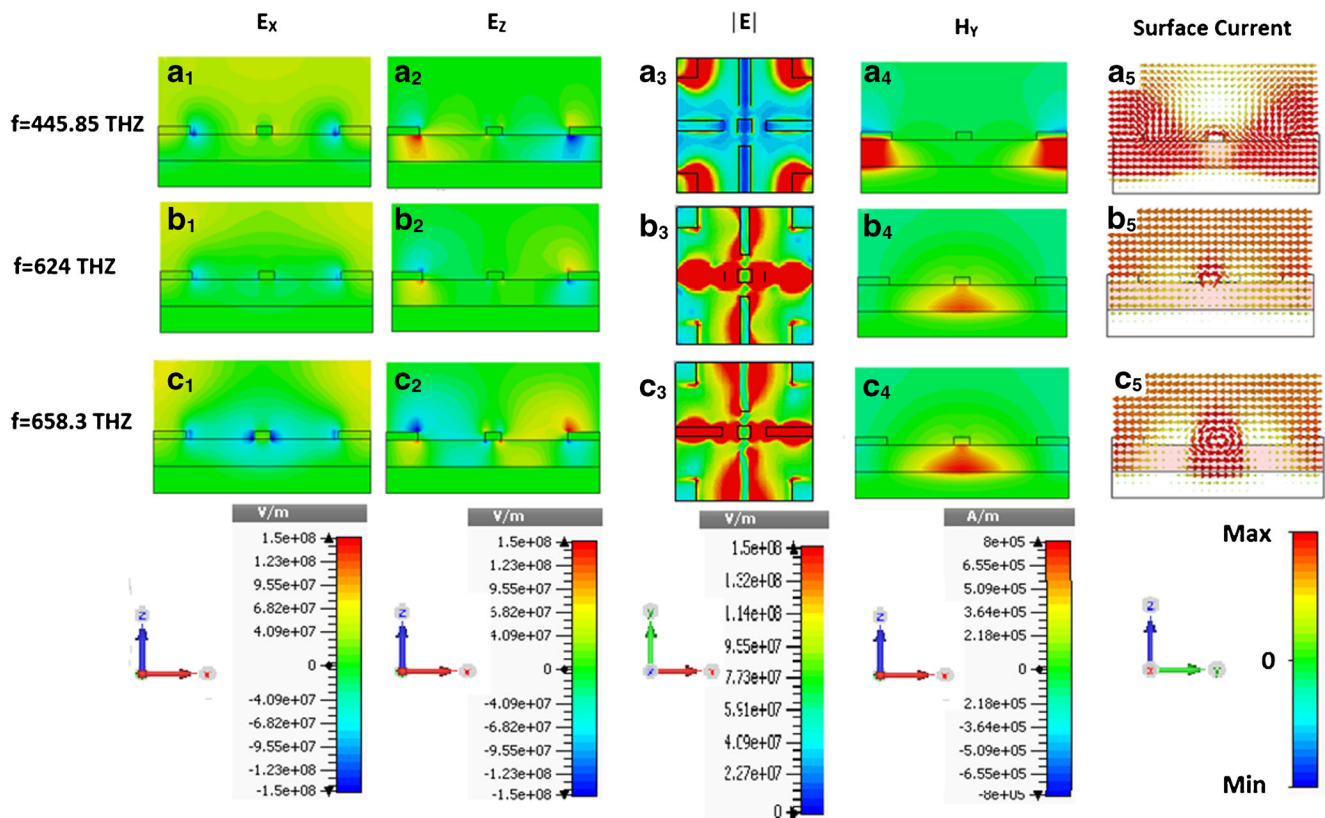


**Fig. 5** ( $a_1$ – $c_1$ )  $X$ -component of the electric field distributions of proposed absorber at  $f=445.85$  THz,  $f=624$  THz, and  $f=658.3$  THz, respectively. ( $a_2$ – $c_2$ )  $Z$ -component of the electric field distributions of proposed absorber at  $f=445.85$  THz,  $f=624$  THz, and  $f=658.3$  THz, respectively. ( $a_3$ – $c_3$ ) Magnitude of the electric field distributions on the dielectric layer of the proposed absorber at  $f=445.85$  THz,  $f=624$  THz,

and  $f=658.3$  THz, respectively. ( $a_4$ – $c_4$ )  $Y$ -component of the magnetic field distributions of proposed absorber at  $f=445.85$  THz,  $f=624$  THz, and  $f=658.3$  THz, respectively. ( $a_5$ – $c_5$ ) Surface current distributions of proposed absorber at  $f=445.85$  THz,  $f=624$  THz, and  $f=658.3$  THz, respectively. The scales of the corresponding distributions are given at the bottom of each group

perfect absorption can be found when the length is adjusted to be  $c=140$  nm.

In addition, the absorption spectra for the variation of the strip width is also presented. As it is obvious from Fig. 6d, the variation of this parameter (parameter  $t$ ), does not affect the first and the third resonances (except  $t=40$  nm). As discussed before, the first and the third resonances are mainly caused from the resonators of the first group (square patches at the corner) while the second resonance is caused by the second group resonators (strips and the central patch). Therefore, the variation of the geometric dimensions of the strips mostly reduces the second resonance.

As discussed in the previous sections, perfect absorption takes place when the effective impedance of the absorber,  $z(w)$ , matches with the impedance of the free space. This condition ensures the zero reflection and transmission of the incident wave.  $z(w)$  is strongly related with the effective permeability,  $\mu(w)$ , and effective permittivity  $\varepsilon(w)$ , of the absorber ( $z(w) = \sqrt{\mu(w)/\varepsilon(w)}$ ). Thus, impedance matching occurs when the electric and magnetic resonances exist simultaneously. The

calculated normalized impedance of the proposed absorber is given in Fig. 7. The real part,  $\text{Re}(z)$ , and imaginary part,  $\text{Im}(z)$ , of the impedance at resonance wavelength are given in the inset of Fig. 7. In order to fulfill the matching condition, the normalized impedance should satisfy the conditions of: the  $\text{Re}(z) \approx 1$  and  $\text{Im}(z) \approx 0$ . At 624 and 658.3 THz, which have more than 99 % absorption rate, the conditions for  $\text{Re}(z)$  and  $\text{Im}(z)$  are satisfied. For the first resonance which has relatively lower absorption strength with respect to the other resonances,  $\text{Re}(z)=1.24$  which is a little bit higher than the matching condition and  $\text{Im}(z)=-0.19$  which is a little bit lower than the matching condition [32–34]. This is mainly because of the relatively higher reflection rate (98.2 % absorption rate) occurred at this resonance.

For the next exploration, under transverse electromagnetic (TEM) polarization mode, the polarization angle  $\theta$  is changed in order to visualize the polarization dependency of the absorber in the visible frequency range. The results are given in Fig. 8. As Fig. 8 represents, the absorber is completely polarization insensitive under TEM mode due to its four folded symmetric design.

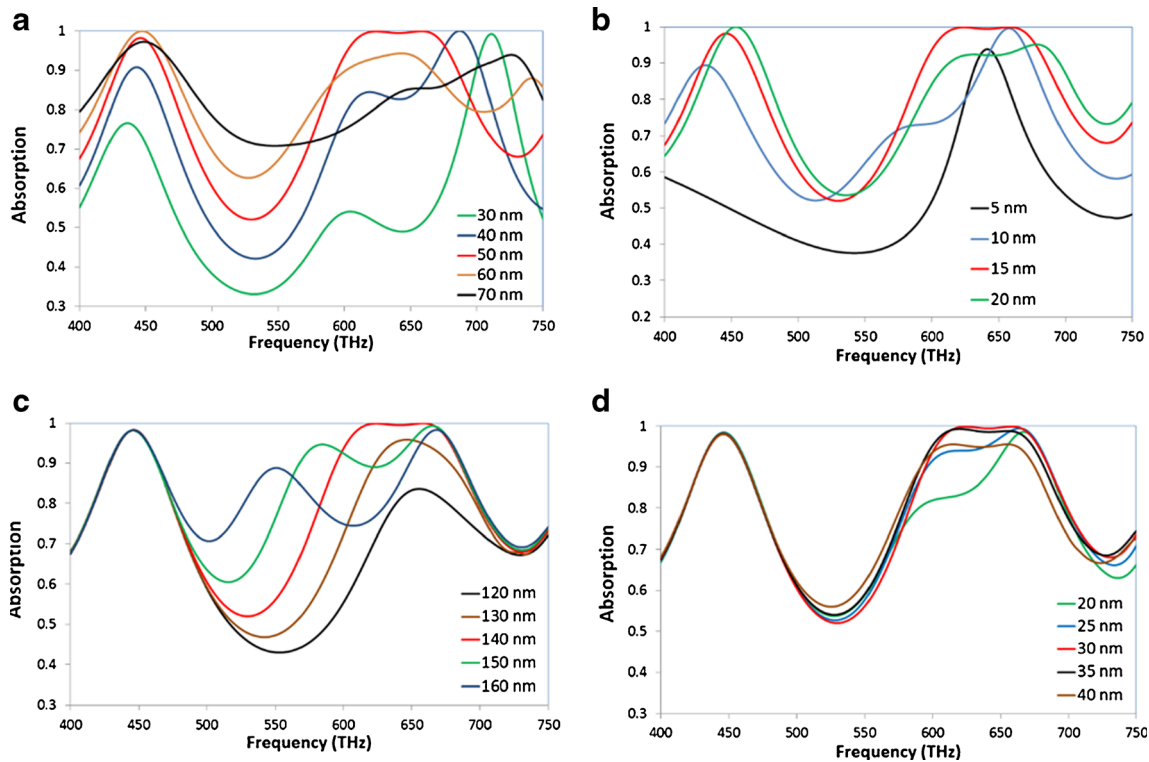


**Fig. 6** Variation of absorption spectra for **a** dielectric layer thickness (parameter  $d$ ), **b** resonator thickness (parameter  $e$ ), **c** strip length (parameter  $c$ ), **d** strip width (parameter  $t$ )

**Theoretical Investigation**

In this part, verification of the numerical result (given in the previous sections) for the visible frequency range is done by using interference theory model. As given in the inset of Fig. 9, when the wave strikes to the absorber, some of the incident wave are reflected back by layer 1, and some of incident wave are transmitted through the region 1 to region 2. The coefficients of layer 1 are as follows:  $S_{11} = |s_{11}|e^{j\theta_{11}}$ ,  $S_{21} = |s_{21}|e^{j\theta_{21}}$ ,  $S_{12} = |s_{12}|e^{j\theta_{12}}$ , and  $S_{22} = |s_{22}|e^{j\theta_{22}}$ . Here,  $S_{11}$  gives the reflection coefficient from region 1 to region 1,  $S_{21}$

represents transmission coefficient from region 1 to region 2,  $S_{12}$  represents transmission coefficient from region 1 to region 2, and  $S_{22}$  represents the reflection coefficient from region 2 to region 2. According to these coefficients, the extended interference model, which calculates the total  $S_{11}$  parameter, is given in Eq. 4 [35].

$$\Sigma S_{11} = S_{11} + S_{12}e^{-j(2\beta+\pi)}S_{21} + S_{12}e^{-j(2\beta+\pi)}(S_{22}e^{-j(2\beta+\pi)})S_{12} + S_{12}e^{-j(2\beta+\pi)}(S_{22}e^{-j(2\beta+\pi)})^2 + \dots \tag{4}$$

Here,  $\beta$  is the complex propagation phase.  $\beta = kd$  where  $k$  and  $d$  represent the wavenumber in region 2 and the propagation distance of the transmitting wave from layer 1,

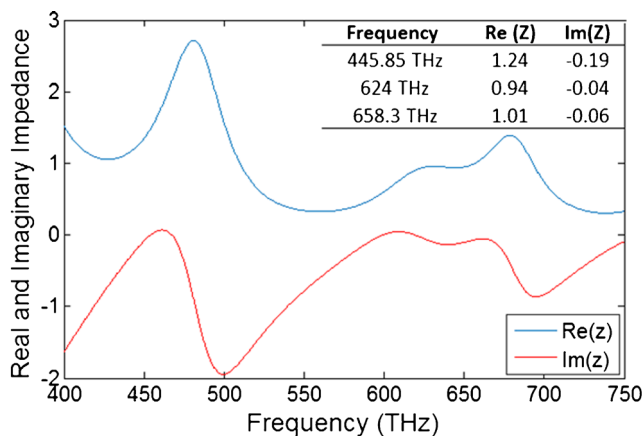


**Fig. 7** Normalized effective impedance of the absorber. The inner table shows the real and imaginary parts of the impedance at resonant frequencies

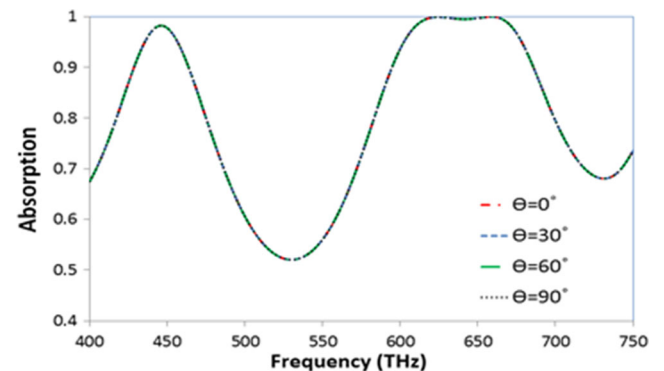


**Fig. 8** The absorption spectra under for various polarization angles

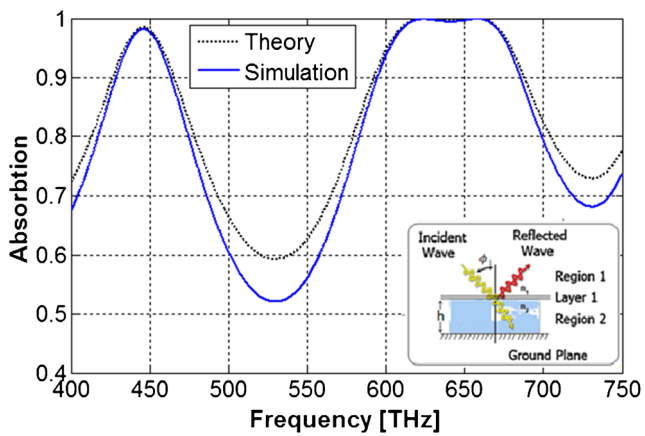


**Fig. 9** Comparison of the theoretical and simulation results for absorption [35]

respectively. Note that the wavenumber  $d$  here is different from “parameter  $d$ ” used in the previous section.

As the main operation frequency range is defined to be visible range, the theoretical calculation is carried out only in this range. The theoretical and numerical results are compared in Fig. 9. According to Fig. 9, it can be commented on that the numerical and theoretical results are in a good agreement, especially around the resonances.

## Conclusion

In conclusion, in this work, a metamaterial absorber design formed by the combination of the three effective layers is introduced. Unlike the most of the studies based on multiple layers presented in the literature, the combination of only three layers are used to obtain the multiple and wide-band perfect absorption. The characterization of the multiband resonances is carried out by identifying the responses of each resonators and discovering the origins by using the electric and magnetic field distributions at resonant frequencies. The investigation of the dependency of the geometric parameters on the metamaterial absorber is also presented. As a conclusion, the introduced polarization insensitive, multiband metamaterial absorber can be used for the harvesting of solar energy, sensing applications, absorption of solar radiation, detection, and imaging in the solar spectrum.

**Acknowledgments** The work reported here was carried out at Middle East Technical University—Northern Cyprus Campus (METU-NCC). It is supported by METU-NCC under the grant number of BAP-FEN-15-D-3.

## References

- Ziolkowski RW (2003) Design, fabrication, and testing of double negative metamaterials. *IEEE Trans Antennas Propag* 51:1516–1529
- Engheta N, Ziolkowski RW (2005) A positive future for double-negative metamaterials. *IEEE Trans Microw Theory Tech* 53:1535–1556
- Yu Z, Liu S, Fang C, Huang X, Yang H (2015) Design, simulation, and fabrication of single-/dual-/triple band metamaterial absorber. *Phys Scr* 90:065501
- Li W, Zhou X, Ying Y, Qiao X, Qin F, Li Q, Che S (2015) Polarization-insensitive wide-angle multiband metamaterial absorber with a double layer modified electric ring resonator array. *AIP Advances* 5:067151
- Dincer F, Karaaslan M, Unal E, Delihacioglu K, Sabah C (2014) Design of polarization and incident angle insensitive dual-band metamaterial absorber based on isotropic resonator. *Prog Electromagn Res* 144:123
- He X, Yan S, Ma Q, Zhang Q, Jia P, Wu F, Jiang J (2015) Broadband and polarization-insensitive terahertz absorber based on multilayer metamaterials. *Opt Commun* 340:44
- Wang B, Zhai X, Wang G, Huang W, Wang L (2015) Frequency tunable metamaterial absorber at deep-subwavelength scale. *Opt Mater Express* 5:227
- Cong L, Tan S, Yahiaoui R, Yan F, Zhang W, Singh R (2015) Experimental demonstration of ultrasensitive sensing with terahertz metamaterial absorbers: a comparison with the metasurfaces. *Appl Phys Lett* 106:031107
- Ayas S, Bakan G, Dana A (2015) Rounding corners of nano-square patches for multispectral plasmonic metamaterial absorbers. *Opt Express* 23:11763
- Wang H, Wang L (2013) Perfect selective metamaterial solar absorbers. *Opt Express* 21:A1078
- Mulla B, Sabah C (2015) Perfect metamaterial absorber design for solar cell applications. *Waves Random Complex Media* 25:382
- Diaz-Rubio A, Hibbins AP, Carbonell J, Sánchez-Dehesa J (2015) Experimental verification of total absorption by a low-loss thin dielectric layer. *Appl Phys Lett* 106:241604
- Pendry JB, Schurig D, Smith DR (2006) Controlling electromagnetic fields. *Sci* 312:1780
- Cai W, Genov DA, Shalaev VM (2005) Superlens based on metal-dielectric composites. *Phys Rev B* 72:193101
- Landy NI, Sajuyigbe S, Mock JJ, Smith DR, Padilla WJ (2008) Perfect metamaterial absorber. *Phys Rev Lett* 100:207402
- Almoneef TS, Ramahi OM (2015) Metamaterial electromagnetic energy harvester with near unity efficiency. *Appl Phys Lett* 106:153902
- Dayal G, Ramakrishna SA (2013) Design of multi-band metamaterial perfect absorbers with stacked metal–dielectric disks. *J Opt* 15:055106
- Rufangura P, Sabah C (2015) Dual-band perfect metamaterial absorber for solar cell applications. *Vacuum* 120:68
- Maier T, Brueckl H (2006) Microbolometers for the mid infra-red. *Opt. Lett* 35:3766
- Liu N, Mesch M, Weiss T, Hentschel M, Giessen H (2010) Infrared perfect absorber and its application as plasmonic sensor. *Nano Lett* 10:2342
- Wu C, Neuner B III, John J, Milder A, Zollars B, Savoy S, Shvets G (2012) Metamaterial-based integrated plasmonic absorber/emitter for solar thermo-photovoltaic systems. *J Opt* 14:024005
- Cui Y, He Y, Jin Y, Ding F, Yang L, Ye Y, Zhong S, Lin Y, He S (2014) Plasmonic and metamaterial structures as electromagnetic absorbers. *Laser Photonics Rev* 8:495
- Huang L, Chen H-T (2013) A, Brief review on terahertz metamaterial perfect absorbers THz. *Sci Tech* 6:26
- Wang J, Fan C, Ding P, He J, Cheng Y, Hu W, Cai G, Liang E, Xue Q (2012) Tunable broad-band perfect absorber by exciting of multiple plasmon resonances at optical frequency. *Opt Express* 20:14871



25. Watts CM, Liu X, Padilla WJ (2012) Metamaterial electromagnetic wave absorbers. *Adv Mater* 24:OP98
26. Corey Shemelya, Dante DeMeo, Nicole Pfister Latham, Xueyuan Wu, Chris Bingham, Willie Padilla, and Thomas E. Vandervelde
27. Boriskina SV, Ghasemi H, Chen G (2013) Plasmonic materials for energy: from physics to applications. *Mater Today* 16:376
28. Liu K, Jiang S, Ji D, Xie Z, Zhang N, Song H, Xu Y, Gan Q (2015) Super absorbing ultraviolet metasurface. *IEEE Photonics Technol Lett* 27:1539
29. Liang Q, Yu W, Zhao W, Wang T, Zhao J, Zhang H, Tao S (2013) Numerical study of the meta-nanopyramid array as efficient solar energy absorber. *Opt Mater Express* 3:1187
30. Jun Wu, Changhe Zhou, Junjie Yu, Hongchao Cao Shubin Li, Wei Jia (2014) TE polarization selective absorber based on metal-dielectric grating structure for infrared frequencies. *Opt commun* 329:3831. E. D Palik. Handbook of optical constant of solids. San Diego (CA): Academic Press; 1985
- 31.
32. Huang L, Chen H (2011) Multi-band and polarization insensitive metamaterial absorber. *Prog electromagn Res* 113:103
33. Lee H-M, Lee HS (2013) A metamaterial based microwave absorber composed of coplanar electric-field-coupled resonator and wire array. *Prog Electromagn Res C* 34:111
34. Wang JF, Qu SB, Fu ZT, Ma H, Yang YM, Wu X (2009) Three-dimensional metamaterial microwave absorbers composed of coplanar magnetic and electric resonators. *Prog Electromagn Res* 7:24
35. Dincer F, Karaaslan M, Unal E, Akgol O, Sabah C (2014) Design of polarization- and incident angle-independent perfect metamaterial absorber with interference theory. *J Electron Mater* 43:3949